Revisiting Linear Stability Analysis of Plane Couette Flow with Rarefaction Effects using BGK-LSE

Research Project - 00850851

Mor Aharoni | 319057568
Advisor: Prof. vassilis theofilis

Department of Aerospace Engineering
Technion – Israel Institute of Technology

Spring 2025

1 Introduction

This work applies the method proposed in "A novel linear stability analysis method for plane Couette flow considering rarefaction effects" (Zou et al., 2023) to the BGK-LSE framework. We consider a flow bounded by two infinite parallel plates, which move in opposite directions at the same speed, U_w^*. The plates are located at $y^* = \pm H/2$, where H is the distance between them, as illustrated in Figure 1. The coordinate x^* denotes the longitudinal direction along the channel centerline, and y^* denotes the normal direction, perpendicular to the walls.[1]

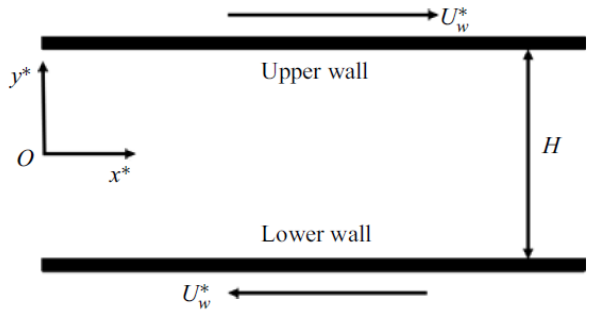

Figure 1: Schematic of the plane Couette flow

This project addresses the challenge of solving the integrodifferential equation that governs this system. This physical problem is defined across four dimensions: the spatial coordinate y, two microscopic velocity coordinates, ξ_x and ξ_y, and time. Time will be used to decompose the variables into two components: a steady base flow term and an unsteady perturbation term. The methodology presented here utilizes spectral methods to solve a simplified Laplace equation problem. This fundamental numerical basis is essential for my ongoing master's degree research, which aims to solve the primary integrodifferential equation.

2 Theoretical Background

2.1 The Governing Equations

The Boltzmann equation is defined as[2]:

$$\frac{\partial f^*}{\partial t^*} + \boldsymbol{\xi}^* \cdot \frac{\partial f^*}{\partial \boldsymbol{x}^*} + \frac{\boldsymbol{X}_\mathbf{0}^*}{m^*} \cdot \frac{\partial f^*}{\partial \boldsymbol{\xi}^*} = \int (f^{*\prime} f^{*\prime}_1 - f^* f_1^*) g b \mathrm{d}b \mathrm{d}\varepsilon \mathrm{d}\boldsymbol{\xi}_\mathbf{1} \tag{1}$$

where:

$$f^* = f^*(t^*, \boldsymbol{x}^*, \boldsymbol{\xi}^*), \quad f^{*\prime} = f^{*\prime}(t^*, \boldsymbol{x}^*, \boldsymbol{\xi}^{*\prime}), \quad f_1^* = f_1^*(t^*, \boldsymbol{x}^*, \boldsymbol{\xi}_1^*), \quad f_1^{*\prime} = f_1^{*\prime}(t^*, \boldsymbol{x}^*, \boldsymbol{\xi}_1^{*\prime})$$

The integral on the right side is called the collision integral, and the primes denote the velocity of the molecules after the collision. "That equation is the fundamental equation of the kinetic theory of gases" (Kogan, 1969). It describes how the distribution of gas particles in space evolves as a result of free motion and collisions. The BGK model is an approximate form of the Boltzmann equation introduced to simplify the collision integral and make the equation more solvable.[3] The BGK approximation of the Boltzmann equation for a two-dimensional flow is expressed as:

$$\frac{\partial f^*}{\partial t^*} + \boldsymbol{\xi}^* \cdot \boldsymbol{\nabla}^* f^* = \frac{1}{\tau^*} \left(f^{e*} - f^* \right) \tag{2}$$

where f^* is the distribution function and f^{e*} is the local Maxwellian equilibrium distribution, defined for a three-dimensional velocity space ($D = 3$) as:

$$f^{e*} = \frac{\rho^*}{(2\pi R T^*)^{D/2}} \exp\left(-\frac{|\boldsymbol{\xi}^* - \boldsymbol{u}^*|^2}{2RT^*} \right) \tag{3}$$

The parameter τ^* is the relaxation time, which is defined as the mean time between particle collisions.[3] The analysis relies on the following assumptions:

- The base flow is fully developed ($\bar{v} = 0$, $\frac{\partial \bar{u}}{\partial x} = 0$).
- The flow is isothermal ($T = \text{const.}$).
- The fluid follows the hard-sphere molecular model ($\omega = 0.5$), which decouples temperature and collision cross-section area.

2.2 Scaling Relations

The characteristic reference scales used for non-dimensionalization are summarized in Table 1. A superscript $(\cdot)^*$ denotes a dimensional quantity, while a non-superscript symbol represents the corresponding dimensionless quantity.

Variable	**Reference Scale**	**Physical Quantity**
L_{ref}	$\frac{h}{2}$	Characteristic Length
U_{ref}	$\sqrt{2RT}$	Reference Velocity
μ_{ref}	$\rho_{\text{ref}} U_{\text{ref}} L_{\text{ref}}$	Dynamic Viscosity Scale
T_{ref}	T_{ref}	Temperature Scale
p_{ref}	$\rho_{\text{ref}} U_{\text{ref}}^2$	Pressure Scale
t_{ref}	$\frac{L_{\text{ref}}}{U_{\text{ref}}}$	Time Scale
τ_{ref}	$\frac{\mu_{\text{ref}}}{p_{\text{ref}}}$	Relaxation Time Scale

Table 1: Reference quantities used for non-dimensionalization

Using the reference quantities from Table (1), the normalized isothermal state equation is:

$$p = \frac{1}{2}\rho \tag{4}$$

The reference pressure and temperature are selected as the freestream conditions ($p_{\text{ref}} = p_\infty, T_{\text{ref}} = T_\infty$).
The viscosity–temperature relation is given by the power law:

$$\mu^* = \mu_\infty \left(\frac{T}{T_\infty}\right)^\omega \tag{5}$$

where μ_∞ is the viscosity under freestream conditions. The mean free path can be written as (Shen, 2006)[4]:

$$\lambda_{ref} = \frac{2\mu_\infty(5-2\omega)(7-2\omega)}{15\rho_{ref}(2\pi R T_{ref})^{\frac{1}{2}}} \tag{6}$$

Substituting $\omega = 0.5$ for the hard sphere model into Equation (6) and using the reference quantities from Table (1) yield the dimensionless viscosity:

$$\mu = \frac{5\sqrt{\pi}\text{Kn}}{16} \tag{7}$$

where the Knudsen number is defined as:

$$\text{Kn} = \frac{\lambda_{\text{ref}}}{L_{\text{ref}}} \tag{8}$$

Finally, using the normalized isothermal state equation from Equation (4) and dividing the viscosity by the pressure, we obtain the dimensionless relaxation time:

$$\tau = \frac{5\sqrt{\pi}\text{Kn}}{8\rho} \tag{9}$$

Introducing the non-dimensional form of the Maxwellian distribution, we define the dimensionless equilibrium distribution f^e:

$$f^{e*} = \frac{\rho_\infty}{{U_{th}^*}^3} \overbrace{\rho\pi^{-\frac{3}{2}} \exp\left\{-|\boldsymbol{\xi} - \boldsymbol{u}|^2\right\}}^{f^e} \longrightarrow f^{e*} = \frac{\rho_\infty}{{U_{th}^*}^3} f^e \tag{10}$$

By substituting the reference quantities and the dimensionless relaxation time from Equation (9) into the BGK equation, we obtain the dimensionless two-dimensional isothermal BGK equation:

$$\frac{\partial f}{\partial t} + \xi_x \frac{\partial f}{\partial x} + \xi_y \frac{\partial f}{\partial y} = \frac{8\rho}{5Kn\sqrt{\pi}}(f^e - f) \tag{11}$$

To remove the dependence on the velocity component ξ_z, the distribution function f is integrated over ξ_z, since this is a two-dimensional problem. This yields the reduced distribution function g:

$$g(x, y, \xi_x, \xi_y) = \int_{-\infty}^{\infty} f(x, y, \xi_x, \xi_y, \xi_z)\, d\xi_z \tag{12}$$

Substituting Equation (12) into Equation (11) yields the governing equation for g:

$$\frac{\partial g}{\partial t}+\xi_x\frac{\partial g}{\partial x}+\xi_y\frac{\partial g}{\partial y}=\frac{8\rho}{5Kn\sqrt{\pi}}(g^e-g) \tag{13}$$

where the reduced equilibrium distribution function, g^e, is:

$$g^e=\rho\pi^{-\frac{3}{2}}\exp\Big\{-|\boldsymbol{\xi}-\boldsymbol{u}|^2\Big\} \tag{14}$$

2.3 Linearization

The macroscopic flow variables (ρ,u,v,p) and the distribution functions (g,g^e) are decomposed into a base flow (denoted by an overbar $\bar{(\cdot)}$), which satisfies the BGK equation and an unsteady perturbation (denoted by a tilde $\tilde{(\cdot)}$)[5]:

$$\begin{cases} u=\bar{u}(y)+\tilde{u}(x,y,t)\\ v=\tilde{v}(x,y,t)\\ \rho=\bar{\rho}(y)+\tilde{\rho}(x,y,t)\\ p=\bar{p}(y)+\tilde{p}(x,y,t)\\ g=\bar{g}(y,\xi_x,\xi_y)+\tilde{g}(t,x,y,\xi_x,\xi_y)\\ g^e=\bar{g^e}(y,\xi_x,\xi_y)+\tilde{g^e}(t,x,y,\xi_x,\xi_y) \end{cases} \tag{15}$$

Substituting these perturbations into Equation (13), neglecting second-order terms, and canceling out the base flow terms results in the linearized BGK equation for the perturbation $\tilde{g}$:

$$\frac{\partial\tilde{g}}{\partial t}+\xi_x\frac{\partial\tilde{g}}{\partial x}+\xi_y\frac{\partial\tilde{g}}{\partial y}=\frac{8}{5Kn\sqrt{\pi}}\left[\bar{\rho}\tilde{g^e}+\tilde{\rho}\bar{g^e}-\bar{\rho}\tilde{g}-\tilde{\rho}\bar{g}\right] \tag{16}$$

To define $\bar{g}^e$ and $\tilde{g}^e$, we substitute the perturbations from Equation (15) into the definition of g^e and use a Taylor expansion on the exponential term. This separates the Maxwellian terms into base flow and perturbation components:

$$\begin{cases} \bar{g}^e=\bar{\rho}\pi^{-\frac{3}{2}}e^{-(\xi_x^2-2\xi_x\bar{u}+\bar{u}^2+\xi_y^2)}\\ \tilde{g}^e=\bar{\rho}\pi^{-\frac{3}{2}}\left[e^{-(\xi_x^2-2\xi_x\bar{u}+\bar{u}^2+\xi_y^2)}(-2\bar{u}\tilde{u}+2\xi_x\tilde{u}+2\xi_y\tilde{v})\right]+\tilde{\rho}\pi^{-\frac{3}{2}}e^{-(\xi_x^2-2\xi_x\bar{u}+\bar{u}^2+\xi_y^2)} \end{cases} \tag{17}$$

Thus:

$$\tilde{g}^e=\bar{g}^e\left\{\frac{\tilde{\rho}}{\bar{\rho}}+2\left[(\xi_x-\bar{u})\tilde{u}+\xi_y\tilde{v}\right]\right\} \tag{18}$$

2.4 Harmonic wave perturbations[5]

Let us analyze the system's stability by introducing a harmonic wave perturbation for the state vector $\tilde{q}$:

$$\tilde{q}=[\tilde{\rho}\quad\tilde{u}\quad\tilde{v}\quad\tilde{g}\quad\tilde{g}^e]^T\qquad\tilde{q}=\hat{q}(y)\exp(i(\alpha x-\varpi t)) \tag{19}$$

Here, α is the real wave number and ω is the complex frequency ($\omega=\omega_r+i\omega_i$).
Substituting this harmonic form into the linearized equations, (16) and (18), and dividing the exponential terms $\exp[i(\alpha x-\omega t)]$, we obtain the equations for the amplitude functions:

$$-i\omega\hat{g}+\xi_x i\alpha\hat{g}+\xi_y\frac{\partial\hat{g}}{\partial y}=\frac{8}{5\mathrm{Kn}\sqrt{\pi}}\left[\bar{\rho}\hat{g^e}+\hat{\rho}\bar{g^e}-\bar{\rho}\hat{g}-\hat{\rho}\bar{g}\right]$$

$$\hat{g}^e=\bar{g}^e\left\{\frac{1}{\bar{\rho}}\hat{\rho}+2\left[(\xi_x-\bar{u})\hat{u}+\xi_y\hat{v}\right]\right\}$$

Substituting the expression for $\hat{g}^e$ (Equation (2.4)) into the reduced BGK equation and rearranging terms yields:

$$\left(\xi_x i\alpha+\frac{8\bar{\rho}}{5\mathrm{Kn}\sqrt{\pi}}\right)\hat{g}-\left[\frac{8(\bar{g}^e-\bar{g})}{5\mathrm{Kn}\sqrt{\pi}}+\frac{8\bar{g}^e}{5\mathrm{Kn}\sqrt{\pi}}\right]\hat{\rho}+\xi_y\frac{\partial\hat{g}}{\partial y}-\frac{16\bar{\rho}}{5\mathrm{Kn}\sqrt{\pi}}\bar{g}^e(\xi_x-\bar{u})\hat{u}-\frac{16\bar{\rho}}{5\mathrm{Kn}\sqrt{\pi}}\xi_y\hat{v}=i\omega\hat{g} \tag{20}$$

2.5 Moments

The macroscopic hydrodynamic fields are defined as moments of the distribution function f. For three-dimensional velocity space, these definitions are:

$$\rho = \iiint f \, d\boldsymbol{\xi} \tag{21a}$$

$$u_i = \frac{1}{\rho} \iiint \xi_i f \, d\boldsymbol{\xi} \tag{21b}$$

Using the reduced distribution function g from Equation (12), substituting the perturbations from Equation (15), neglecting higher-order terms, and applying the harmonic wave assumption from Equation (19), the linearized and non-dimensional moment equations become:

$$\hat{\rho} = \iint \hat{g} \, d\xi_x d\xi_y \tag{22a}$$

$$\hat{u} = \frac{1}{\bar{\rho}} \iint \xi_x \hat{g} \, d\xi_x d\xi_y - \frac{\bar{u}}{\bar{\rho}} \hat{\rho} \tag{22b}$$

$$\hat{v} = \frac{1}{\bar{\rho}} \iint \xi_y \hat{g} \, d\xi_x d\xi_y \tag{22c}$$

By substituting Equation (22a) into Equation (22b), the expression for $\hat{u}$ can be simplified:

$$\hat{u} = \frac{1}{\bar{\rho}} \iint (\xi_x - \bar{u}) \hat{g} \, d\xi_x d\xi_y$$

To obtain the final closed equation, we substitute the moment relations (Equations (22)) into the harmonically perturbed BGK equation. This is the equation presented:

$$\begin{aligned} &\left(\xi_x i\alpha + \frac{8\bar{\rho}}{5\mathrm{Kn}\sqrt{\pi}} \right) \hat{g} - \left[\frac{8(\bar{g}^e - \bar{g})}{5\mathrm{Kn}\sqrt{\pi}} + \frac{8\bar{g}^e}{5\mathrm{Kn}\sqrt{\pi}} \right] \int_{-\infty}^{\infty} \int_{-\infty}^{\infty} \hat{g} \, \mathrm{d}\xi_x \, \mathrm{d}\xi_y + \xi_y \frac{\partial \hat{g}}{\partial y} \\ &- \frac{16}{5\mathrm{Kn}\sqrt{\pi}} \bar{g}^e (\xi_x - \bar{u}) \int_{-\infty}^{\infty} \int_{-\infty}^{\infty} (\xi_x - \bar{u}) \hat{g} \, \mathrm{d}\xi_x \, \mathrm{d}\xi_y - \frac{16}{5\mathrm{Kn}\sqrt{\pi}} \bar{g}_e \xi_y \int_{-\infty}^{\infty} \int_{-\infty}^{\infty} \xi_y \hat{g} \, \mathrm{d}\xi_x \, \mathrm{d}\xi_y = i\omega \hat{g} \end{aligned} \tag{23}$$

3 Numerical Operators

3.1 Laplace Eigenvalue Equation

3.1.1 1D Laplace Eigenvalue Equation

The fundamental numerical approach is demonstrated using the 1D Laplace EVP:

$$X'' = \lambda^2 X \tag{24}$$

This equation was solved in the domain $x \in [0, 1]$ subject to mixed homogeneous boundary conditions:

$$X'(0) = 0 \qquad X(1) = 0$$

The analytic solution yields a discrete set of eigenvalues λ_j and corresponding eigenfunctions X_j:

$$\begin{cases} \lambda_j = \frac{\pi}{2}(2j-1) \\ X_j(x) = A \cos\left(\frac{\pi}{2}(2j-1)x\right) \end{cases}, \quad j = 1, 2, 3, \ldots$$

Numerically, the domain was discretized using a Chebyshev-Gauss-Lobatto (CGL) grid (e.g., $N = 32, 64$ points). The EVP was solved using spectral methods, where the differential operator is represented by the differentiation matrix D:

$$D^2\mathbf{X} = \lambda^2 \mathbf{I}\mathbf{X} \quad \longrightarrow \quad \mathbf{A} = D^2, \quad \mathbf{B} = \mathbf{I}$$

3.1.2 2D Laplace Eigenvalue Problem

The method extends to the 2D Laplace EVP in the domain $(x, y) \in [0, 1] \times [0, 1]$:

$$\frac{\partial^2 Z}{\partial x^2} + \frac{\partial^2 Z}{\partial y^2} = \lambda^2 Z \tag{25}$$

This problem was solved subject to homogeneous Dirichlet boundary conditions on all boundaries:

$$Z(x,0) = Z(x,1) = Z(0,y) = Z(1,y) = 0$$

Using the method of separation of variables ($Z(x,y) = X(x)Y(y)$), the 2D problem decouples into two independent 1D EVPs, where the total eigenvalue is $\lambda^2 = \lambda_x^2 + \lambda_y^2$. Since Dirichlet conditions are used, the analytic solutions are based on sine functions, yielding eigenvalues $\lambda_{x,j} = j\pi$ and $\lambda_{y,k} = k\pi$. Numerically, the 2D Laplace operator ∇^2 is constructed using the Kronecker product ($\otimes$):

$$\mathbf{D}_{2D} = (D_x^2 \otimes \mathbf{I}_y) + (\mathbf{I}_x \otimes D_y^2)$$

The numerical 2D EVP is then solved as: $\mathbf{D}_{2D}\mathbf{Z} = \lambda^2\mathbf{Z}$.

3.1.3 3D Laplace Eigenvalue Problem

The final methodology utilizes the 3D Laplace EVP in the domain $(x,y,z) \in [0,1]^3$:

$$\frac{\partial^2 V}{\partial x^2} + \frac{\partial^2 V}{\partial y^2} + \frac{\partial^2 V}{\partial z^2} = \lambda^2 V \tag{26}$$

This problem is solved using homogeneous Dirichlet boundary conditions on all six faces of the unit cube. This is the relevant numerical configuration for the BGK-LSE analysis, which operates in a three-dimensional domain. The 3D discrete Laplace operator ∇^2 is constructed by extending the Kronecker product:

$$\mathbf{D}_{3D} = (D_x^2 \otimes \mathbf{I}_y \otimes \mathbf{I}_z) + (\mathbf{I}_x \otimes D_y^2 \otimes \mathbf{I}_z) + (\mathbf{I}_x \otimes \mathbf{I}_y \otimes D_z^2)$$

The complete 3D EVP is solved as: $\mathbf{D}_{3D}\mathbf{V} = \lambda^2\mathbf{V}$.

3.2 Chebyshev-Gauss-Lobatto Grid[6]

To mitigate Runge's phenomenon oscillations near domain boundaries caused by uniform polynomial interpolation, the Chebyshev-Gauss-Lobatto grid is used. These clustered points provide spectral accuracy and are defined over the domain $x \in [-1,1]$ as:

$$x_j^{CGL} = \cos\left(\frac{j\pi}{N}\right), \quad j = 0,1,\ldots,N \tag{27}$$

where N is the polynomial degree. The CGL grid defines the fundamental elements of the spectral method. The Lagrange basis function $K_j(x)$ and the Chebyshev polynomials of the first kind $T_n(x)$ are given by:

$$K_j(x) = \frac{\omega(x)}{(x-x_j)\omega'(x_j)} = \frac{(-1)^{j+1}(1-x^2)}{c_j N^2 (x-x_j)} T_N'(x), \quad \text{where} \quad c_j = \begin{cases} 2, & j = 0, N \\ 1, & 1 \le j \le N-1, \end{cases} \tag{28}$$

and $T_n(x)$ follows the recurrence $T_{n+1}(x) = 2xT_n(x) - T_{n-1}(x)$. The collocation derivative matrix, $\mathbf{D}^{CGL}$, is explicitly defined as:

$$D_{ij}^{CGL} = \begin{cases} \frac{2N^2+1}{6}, & i = j = 0, \\ -\frac{2N^2+1}{6}, & i = j = N, \\ \frac{x_j}{2(1-x_j^2)}, & i = j,\ 1 \le j \le N-1, \\ \frac{c_i}{c_j}\frac{(-1)^{i-j}}{x_i - x_j}, & i \ne j. \end{cases} \tag{29}$$

Since the CGL grid is restricted to $x \in [-1,1]$, any problem on a physical domain η requires a coordinate transformation $\eta(x)$. The physical derivative matrix $\mathbf{D}(\eta)$ is then obtained by applying the chain rule to $\mathbf{D}^{CGL}$:

$$\mathbf{D}(\eta) = \left(\frac{dx}{d\eta}\right) \cdot \mathbf{D}^{CGL} \tag{30}$$

Examples include the linear map for wall bounded domains $x \in [a,b]$ and rational Trigonometric mapping for infinite domains $x \in [-\infty, \infty)$.

3.3 Integral Operator using Chebyshev Quadrature[7]

To solve the main problem numerically, we define an integral operator using a highly accurate quadrature method. The integral over the range $[a, b]$ is approximated using the following discrete relation:

$$\int_a^b f(y)dy = \sum_{j=0}^{N} W(y_j)f(y_j) \tag{31}$$

where $W(y_j)$ represents the Chebyshev weight function corresponding to the node y_j. The weight function $W(y_j)$ is explicitly defined by the summation:

$$W(y_j) = \frac{b_j}{N}\sum_{n=0}^{N} c_n \cos\left(\frac{nj\pi}{N}\right)\int_{-1}^{1} T_n(y)\frac{d\hat{y}}{dy}dy \tag{32}$$

3.4 Discretizations

To numerically solve the integro-differential equation from Equation (23), the derivative and integrals are replaced by their corresponding discrete operators. The integral operator $\iint(\cdot)\, d\xi_x d\xi_y$ is replaced by a summation using a numerical quadrature scheme, where $W_i W_j$ are the associated weights and i, j are indices corresponding to the discretization points of the velocity space. The spatial derivative $\frac{\partial}{\partial y}$ is replaced by a differential matrix D_y.

$$\begin{aligned}\left(\xi_x i\alpha + \frac{8\bar{\rho}}{5\mathrm{Kn}\sqrt{\pi}}\right)\hat{g} - \left[\frac{8(\bar{g}^e - \bar{g})}{5\mathrm{Kn}\sqrt{\pi}} + \frac{8\bar{g}^e}{5\mathrm{Kn}\sqrt{\pi}}\right]\sum_{i=1}^{P}\sum_{j=1}^{Q} W_i W_j \hat{g} + \xi_y D_y \hat{g} \\ - \frac{16}{5\mathrm{Kn}\sqrt{\pi}}\bar{g}^e(\xi_x - \bar{u})\sum_{i=1}^{P}\sum_{j=1}^{Q} W_i W_j(\xi_x - \bar{u})\hat{g} - \frac{16}{5\mathrm{Kn}\sqrt{\pi}}\bar{g}_e\xi_y\sum_{i=1}^{P}\sum_{j=1}^{Q} W_i W_j \xi_y \hat{g} = i\omega\hat{g}\end{aligned} \tag{33}$$

This equation is recast as an eigenvalue problem of the form $A\hat{g} = B\hat{g}$, where $\hat{g}$ is the state vector. By factoring out $\hat{g}$ from the left-hand side and defining the remaining coefficients as operators or matrices:

$$\begin{aligned}\boldsymbol{A} = \left(\xi_x i\alpha + \frac{8\bar{\rho}}{5\mathrm{Kn}\sqrt{\pi}}\right) - \left[\frac{8(\bar{g}^e - \bar{g})}{5\mathrm{Kn}\sqrt{\pi}} + \frac{8\bar{g}^e}{5\mathrm{Kn}\sqrt{\pi}}\right]\sum_{i=1}^{P}\sum_{j=1}^{Q} W_i W_j + \xi_y D_y \\ - \frac{16}{5\mathrm{Kn}\sqrt{\pi}}\bar{g}^e(\xi_x - \bar{u})\sum_{i=1}^{P}\sum_{j=1}^{Q} W_i W_j(\xi_x - \bar{u}) - \frac{16}{5\mathrm{Kn}\sqrt{\pi}}\bar{g}_e\xi_y\sum_{P=0}^{P}\sum_{j=1}^{Q} W_i W_j \xi_y\end{aligned} \tag{34}$$

$$\boldsymbol{B} = i\omega \tag{35}$$

4 Results

We will use MATLAB to generate and present the resulting graphs, as well as to demonstrate the validation of the solution.

4.1 Laplace Eigenvalue Equation

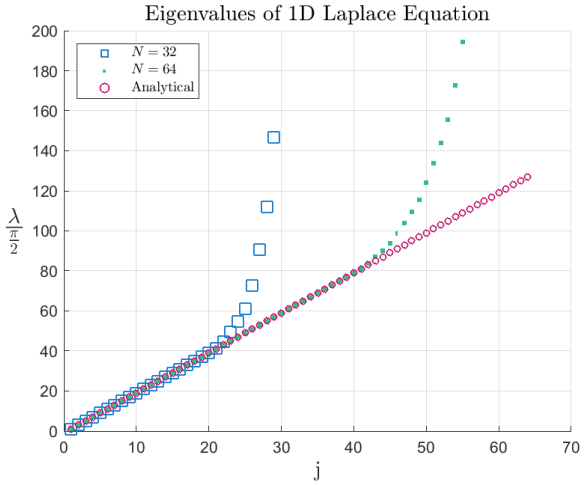

Figure 2: 1D eigenvalue plot

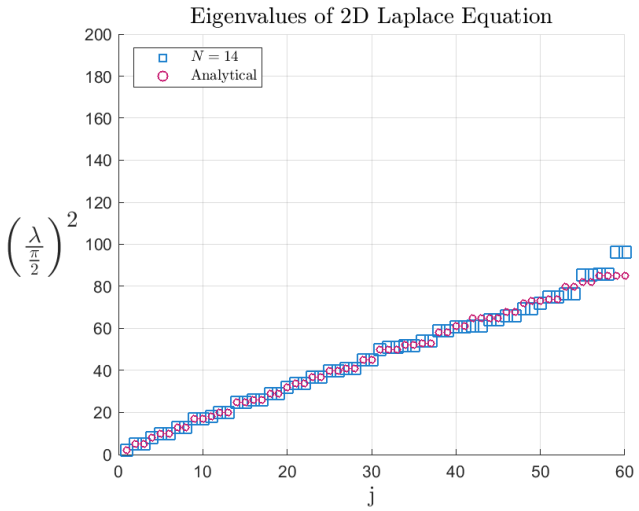

Figure 3: 2D eigenvalue plot

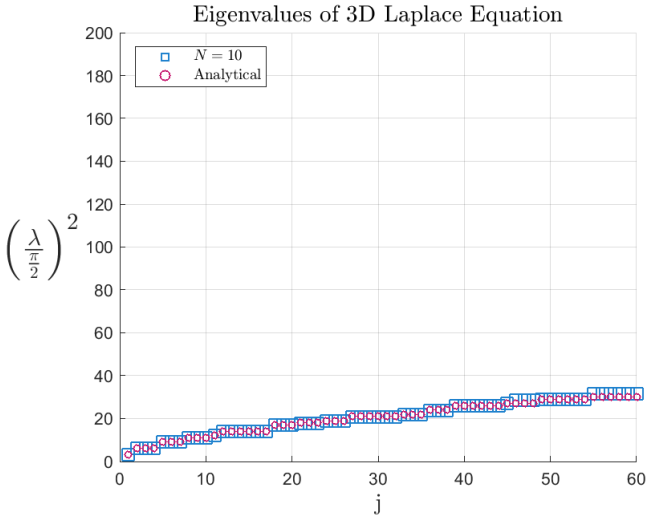

Figure 4: 3D eigenvalue plot

At smaller eigenvalues, the numerical and analytical solutions are compatible and return the same results. However, as the eigenvalues grow larger, a deviation from the analytical solution becomes noticeable.
The figure above illustrates the impact of grid resolution on the accumulated error. Increasing the size of the grid delays the accumulation of numerical errors and eigenvalue divergence, but cannot prevent this phenomenon, and the solution will ultimately diverge.

4.2 Integral Operator using Chebyshev Quadrature

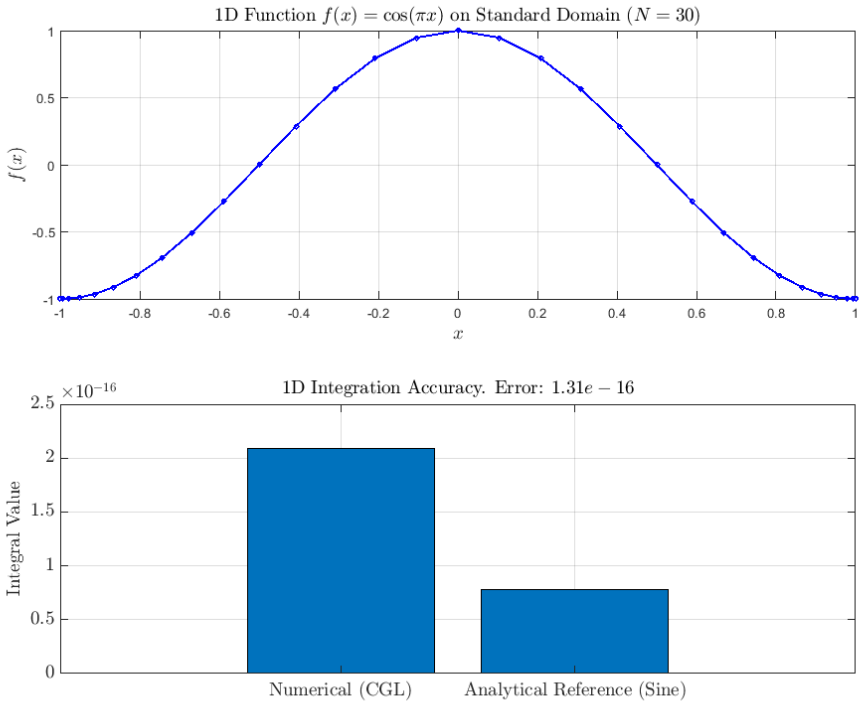

Figure 5: 1D integral plot

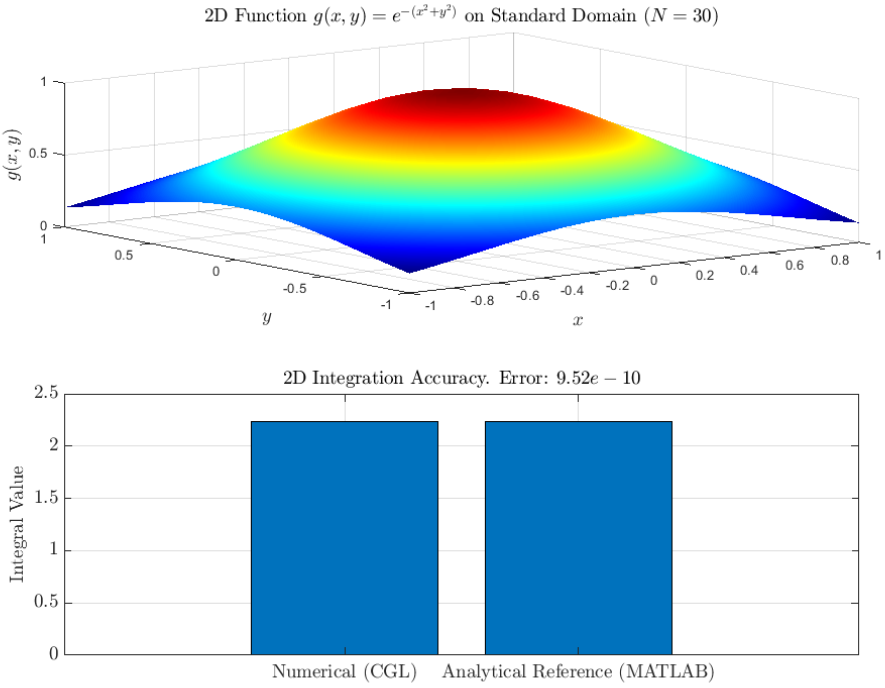

Figure 6: 2D integral plot

As you can see in the figures, the error is very small, indicating that the operator performs with high accuracy.

5 Summary

This research investigates the stability of Plane Couette Flow by using the BGK-LSE model. The main challenge is solving a complex three-dimensional equation. Our approach establishes a powerful numerical foundation using spectral methods to accurately model related physics. By carefully adapting the method to different physical spaces using coordinate transformations, we confirmed that our integral and derivative tools work with extremely high accuracy.

References

[1] S. Zou, L. Bi, C. Zhong, X. Yuan, and Z. Tang, "A novel linear stability analysis method for plane couette flow considering rarefaction effects," *Journal of Fluid Mechanics*, vol. 963, 2023.

[2] M. N. Kogan, *Rarefied Gas Dynamics*. Cambridge, Massachusetts: Springer Science+Business Media, LLC, 1969. Translated from the Russian edition (Nauka Press, Moscow, 1967).

[3] A. Manela, "Lecture notes: Introduction to rarefied gas dynamics." Lecture notes, Technion – Israel Institute of Technology, 2025. Course 00860385, Winter 2025.

[4] C. Shen, "Rarefied gas dynamics: Fundamentals, simulations and micro flows.," *Springer Science & Business Media.*, 2006.

[5] M. P. Juniper, A. Hanifi, and V. Theofilis, "Modal stability theory lecture notes from the flow-nordita summer school on advanced instability methods for complex flows, stockholm, sweden, 2013," *Applied Mechanics Reviews*, vol. 66, 2014.

[6] J. P. Boyd, *Chebyshev and Fourier Spectral Methods*. Mineola, New York: Dover Publications, second ed., 2000.

[7] P. Paredes, *Advances in global instability computations: from incompressible to hypersonic flow*. Doctoral thesis, Escuela Técnica Superior de Ingenieros Aeronáuticos, Universidad Politécnica de Madrid, Madrid, March 2014.

[8] S. A. Schaaf and P. L. Chambre, *Flow of Rarefied Gases*. Princeton, New Jersey: Princeton University Press, 1961.